Nanoscale Control of the Morphology of Lithium Manganate and Silica Composites Using Self-Organized Sol−Gel Media

Brett Ammundsen,† Deborah J. Jones, and Jacques Rozière*

Laboratoire des Agrégats Moléculaires et Matériaux Inorganiques, ESA CNRS 5072, Université Montpellier 2, Place Eugène Bataillon, 34095 Montpellier Cédex 5, France

Gary R. Burns*

School of Chemical and Physical Sciences, Victoria University of Wellington, P.O. Box 600, Wellington, New Zealand

Received August 14, 1997[⊗]

Tetraethoxysilane-derived silica containing lithium and manganese nitrates has been prepared in solutions of poly(oxyethylene) surfactants, giving novel monolithic gels in which the metal ions are associated with the incorporated surfactant. Calcination produces nanocrystalline lithium manganate in the silica matrix. The gels and calcined phases have been characterized by X-ray diffraction and X-ray absorption near edge and extended fine structure spectroscopy at the Mn K-edge (XANES and EXAFS). At 400 °C the reaction between lithium and manganese is incomplete, and both nanocrystalline lithium manganate and disordered manganese in a lower-valent state are identified. Including excess lithium in the gels and calcining at 500 °C allows practically all the manganese in the gels to be reacted to form lithium manganate phases with manganese in a predominantly tetravalent oxidation state. Electron microscopy shows that different microstructures and particle morphologies are obtained by varying the nature and concentration of the poly(oxyethylene) agent. The method therefore not only provides a means of preparing the ternary lithium manganate phase in silica but offers new possibilities for exploiting the self-assembly properties of surfactants to produce composite materials with tailored microstructures.

Introduction

Ternary oxides of lithium and manganese have been extensively studied over the past 15 years as lithium insertion compounds.[1−32] In particular, lithium manganates having the spinel structure have attracted much interest as cyclable lithium-insertion electrodes[1−19] and for their high capacity to selectively sorb lithium ions from natural waters.[23−27] A number of studies have focused on the structural chemistry of the spinel lithium manganates[4,9,10] and on mechanisms of lithium extrac-

† On leave from the School of Chemical and Physical Sciences, Victoria University of Wellington.

⊗ Abstract published in *Advance ACS Abstracts,* November 15, 1997.

(1) Thackeray, M. M.; David, W. I. F.; Bruce, P. G.; Goodenough, J. B. *Mater. Res. Bull.* **1983**, *18*, 461.
(2) Thackeray, M. M.; Johnson, P. J.; de Picciotto, L. A.; Bruce, P. G.; Goodenough, J. B. *Mater. Res. Bull.* **1984**, *19*, 179.
(3) David, W. I. F.; Thackeray, M. M.; de Picciotto, L. A.; Goodenough, J. B. *J. Solid State Chem.* **1987**, *67*, 316.
(4) de Kock, A.; Rossouw, M. H.; de Picciotto, L. A.; Thackeray, M. M.; David, W. I. F.; Ibberson, R. M. *Mater. Res. Bull.* **1990**, *25*, 657.
(5) Ohzuku, T.; Kitagawa, M.; Hirai, T. *J. Electrochem. Soc.* **1990**, *137*, 769.
(6) Tarascon, J. M.; Wang, E.; Shokoohi, F. K.; McKinnon W. R.; Colson, S. *J. Electrochem. Soc.* **1991**, *138*, 2859.
(7) Guyomard, D.; Tarascon, J. M. *J. Electrochem. Soc.* **1992**, *139*, 937.
(8) Pistoia, G.; Wang, G.; Wang, C. *Solid State Ionics* **1992**, *58*, 285.
(9) Thackeray, M. M.; de Kock, A.; Rossouw, M. H.; Liles, D. C.; Bittihn, R.; Hoge, D. *J. Electrochem. Soc.* **1992**, *139*, 363.
(10) Thackeray, M. M.; de Kock, A.; David, W. I. F. *Mater. Res. Bull.* **1993**, *28*, 1041.
(11) Gummow, R. J.; de Kock, A.; Thackeray, M. M. *Solid State Ionics* **1994**, *69*, 59.
(12) Tsumura, T.; Shimizu, A.; Inagaki, M. *J. Mater. Chem.* **1993**, *3*, 995.
(13) Tarascon, J. M.; McKinnon, W. R.; Coowar, F.; Bowmer, T. N.; Amatucci, G.; Guyomard, D. *J. Electrochem. Soc.* **1994**, *141*, 1421.
(14) Barker, J.; West, K.; Saïdi, Y.; Pynenburg, R.; Zachau-Christiansen, B.; Koksbang, R. *J. Power Sources* **1995**, *54*, 475.
(15) Saïdi, M. Y.; Barker, J.; Koksbang, R. *Electrochim. Acta* **1996**, *41*, 199.
(16) Sahaya Prabaharan, S. R.; Siluvai Michael, M.; Prem Kumar, T.; Mani, A.; Athinarayanaswamy, K.; Gangadharan, R. *J. Mater. Chem.* **1995**, *5*, 1035.
(17) Gao, Y.; Reimers, J. N.; Dahn, J. R. *Phys. Rev. B* **1996**, *54*, 3878.
(18) Barker, J.; Koksbang, R.; Saïdi, M. Y. *Solid State Ionics* **1995**, *82*, 143.
(19) Koksbang, R.; Barker, J.; Saïdi, M. Y.; West, K.; Zachau-Christiansen, B.; Skaarup, S. *Solid State Ionics* **1996**, *83*, 151.
(20) Hunter, J. C. *J. Solid State Chem.* **1981**, *39*, 142.
(21) Mosbah, A.; Verbaère, A.; Tournoux, M. *Mater. Res. Bull.* **1983**, *18*, 1375.
(22) Shen, X.-M.; Clearfield, A. J. *J. Solid State Chem.* **1986**, *64*, 270.
(23) Leont'eva, G. V.; Chirkova, L. G. *Zh. Prikl. Khim.* **1988**, *61*, 734.
(24) Ooi, K.; Miyai, Y.; Katoh, S.; Maeda, H.; Abe, M. *Langmuir* **1989**, *5*, 150.
(25) Ooi, K.; Miyai, Y.; Katoh, S.; Maeda, H.; Abe, M. *Langmuir* **1990**, *6*, 289.
(26) Ooi, K.; Miyai, Y.; Sakakihara, J. *Langmuir* **1991**, *7*, 1167.
(27) Feng, Q.; Kanoh, H.; Miyai, Y.; Ooi, K. *Langmuir* **1992**, *8*, 1861.
(28) Ammundsen, B.; Burns, G. R.; Jones, D. J.; Rozière, J. *Chem. Mater.* **1995**, *7*, 2151.
(29) Ammundsen, B.; Aitchison, P. B.; Burns, G. R.; Jones, D. J.; Rozière, J. *Solid State Ionics* **1997**, *97*, 269.
(30) Ammundsen, B.; Burns, G. R.; Jones, D. J.; Rozière, J. *Chem. Mater.* **1996**, *8*, 2799.
(31) Kanoh, H.; Feng, Q.; Miyai, Y.; Ooi, K. *J. Electrochem Soc.* **1993**, *140*, 3162.
(32) Kanoh, H.; Feng, Q.; Miyai, Y.; Ooi, K. *J. Electrochem Soc.* **1995**, *142*, 702.

S0897-4756(97)00569-3 CCC: $14.00 © 1997 American Chemical Society

tion and insertion in the manganese−oxygen framework.[2,20−30] These studies have demonstrated that both electron transfer and lithium−proton exchange can occur, depending on the manganese oxidation state and occupation of octahedral (16d) sites in the spinel.[26−30]

The rate-determining step for lithium insertion reactions in spinel manganese oxide is the diffusion of lithium in the interstitial channels of the crystal.[12,32] Several methods have therefore been proposed to prepare highly divided lithium manganate with low crystallinity and high surface area to improve the lithium insertion and diffusion characteristics.[6,12,16] We have previously suggested that a microemulsion gel method[33,34] may be used to prepare finely divided lithium manganate supported in silica. Such composite materials could have potential applications as filter materials for lithium sorption from geothermal brine or seawater.[35] They might also be used in lithium batteries where lithium-doped silica can behave as a solid lithium electrolyte.[36] The microemulsion gel method involves the hydrolysis of tetraethoxysilane (TEOS) in a combination of aqueous solution, hydrocarbon, and surfactant to produce isotropic silica sols and gels. Precursor solutions stabilized with nonionic poly(oxyethylene) surfactants are particularly useful because they are able to solubilize large amounts of hydrated metal nitrate,[37,38] which associates with the surfactant component in the gel.[39] The method therefore provides a means of dispersing high concentrations of inorganic salts in silica gel materials obtained via a sol−gel process. Metal or metal oxide phase can then be formed by calcination.

We have recently described the use of nonionic poly(oxyethylene) surfactants to prepare highly dispersed manganese oxide in silica.[40] In the present paper we show that poly(oxyethylene) surfactants, homogeneously incorporated into the gel from the precursor solution, promote the reaction of manganese and lithium salts and hence give the formation of ternary spinel lithium manganate in silica gel. The electronic states and local environments of the manganese in the different materials have been probed by X-ray absorption spectroscopy at the manganese K-edge to examine the chemical and structural characteristics of the oxide phases. We have also investigated the effects of varying the nature of the poly(oxyethylene) agent on the morphology and dispersion of the metal oxide phase in the silica. Our results show that the self-assembly properties of the surfactants may be exploited to tailor the microstructures of these composite materials.

Experimental Section

Synthesis and Characterization of the Gels. Surfactant-modified gels were prepared following the method previously reported for manganese-doped silica,[40] in which tetraethoxysilane (TEOS, supplied by Aldrich) was combined with surfactant and an acidified aqueous solution (0.1 M HNO_3) of lithium and manganese nitrate. The quantity of lithium and manganese nitrate was varied between 5 and 15 wt % of the total system [metal nitrate + TEOS + water + surfactant], and the Li/Mn molar ratio was varied between 0.5 and 2.0. In a first stage samples were prepared with 30 wt % Simulsol P4 (Seppic), a preparation of poly(oxyethylene) lauryl ether with an average of 4 oxyethylene groups per molecule, which we hereafter denote $C_{12}(EO)_4$. The properties of $C_{12}(EO)_4$ type surfactant in sol−gel systems have been studied in detail,[40,41] and its capacity to solubilize metal nitrates has been established.[37,38] In a second stage two modified surfactants having a similar hydrophilic−lipophilic balance (HLB) to $C_{12}(EO)_4$ were investigated: a poly(oxyethylene) dodecylphenyl ether with an average of 5 oxyethylene groups, which we denote $C_{12}\phi(EO)_5$, and Simulsol A, a poly(oxyethylene) *cis*-9-oleyl ester with an average of 5−6 oxyethylene groups, denoted $C_{17}C{=}O(EO)_5$, both received from Seppic. Gels were also prepared by substituting an equivalent mass of ethylene glycol for the surfactant content. In the surfactant solutions the hydrolysis of the TEOS produced one-phase solutions which formed transparent monolithic gels after storage in sealed vials at 25 °C for a period of 3−6 days. The ethylene glycol solutions were gelled by warming at 40 °C.

Standard ethanolic gels without surfactant were prepared by dissolving nitrate salts in ethanol solutions of TEOS and acidified water (0.1 M HNO_3). The solutions were sealed and gelled by warming at 40 °C for between 20 and 30 h.

Fourteen days after gelation, all samples were allowed to stand exposed to the atmosphere at 25 °C for 30 days, allowing evaporation of ethanol and water. The resulting shrunken monoliths were then calcined in air at temperatures up to 500 °C to give fragmented materials having a dark blue-black glassy appearance. To characterize crystalline phases, X-ray diffraction (XRD) patterns were recorded on powdered samples by multiply scanning on an automated Philips diffractometer using Cu Kα radiation. For scanning electron microscopy (SEM), samples were sputter coated with a thin (15−20 Å) layer of gold−palladium and examined by a JEOL Model JSM6300F microscope using a tungsten point source operated at 15 kV. Metal oxide phase was distinguished from silica by analysis for manganese and silicon using an attached energy-dispersive X-ray detector. Transmission electron microscopy (TEM) and electron diffraction were carried out using a Philips Model EM420 electron microscope. Samples for TEM were ground and dispersed by ultrasonification in acetone, and drops of the acetone suspension were evaporated onto copper grids coated with a thin film of formovar.

X-ray Absorption Measurements. X-ray absorption spectra were recorded in transmission mode on the EXAFS 3 spectrometer at the French synchrotron facility DCI at LURE, using Si 111 (EXAFS) and 311 (XANES) double-crystal monochromators slightly detuned for harmonic rejection. X-ray absorption near edge (XANES) spectra were recorded from ca. 100 eV before the Mn K-edge (6539 eV) to 100 eV after the edge in a 0.3 eV step size and extended X-ray absorption fine structure (EXAFS) spectra in a 1.5 eV step size to 900 eV after the absorption edge. He/Ne-filled ionization chambers were used to measure the incident and transmitted X-ray flux. Energy calibration was carried out prior to all measurements using a 10 μm Mn foil. Powdered samples were diluted in mixtures of boron nitride and Nujol to produce mulls which were pressed between the Parafilm windows of stainless steel holders and maintained at 77 K in a coldfinger cryostat. Samples in solution were measured in a cell having Mylar windows and an adjustable path length.

(33) Friberg, S. E.; Yang, C. C. In *Innovations in Materials Processing Using Aqueous, Colloidal and Surface Chemistry*; Doyle, F. M., Raghaven, S., Somasundaran, P., Warren, G. W., Eds.; The Minerals, Metals and Materials Society: Warrendale, PA, 1988; p 181.

(34) Ammundsen, B.; Burns, G. R.; Amran, A.; Friberg, S. E. *J. Sol-Gel Sci. Technol.* **1994**, *2*, 341.

(35) Burns, G. R.; Kane, C.; Sahasrabudhe, N. In *New Developments in Ion Exchange*; Abe, M., Kataoka, T., Suzuki, T., Eds.; Kodansha and Elsevier: Tokyo, Amsterdam, 1991; p 523.

(36) Ogasawara, T.; Klein, L. C. *J. Sol-Gel Sci. Technol.* **1994**, *2*, 611.

(37) Friberg, S. E.; Amran, A.; Sjöblom, J. *Prog. Colloid Polym. Sci.* **1992**, *88*, 30.

(38) Saeten, J. O.; Fordedal, H.; Skodvin, T.; Sjöblom, J.; Amran, A.; Friberg, S. E. *J. Colloid Interface Sci.* **1992**, *154*, 167.

(39) Jones, S. M.; Amran, A.; Friberg, S. E. *J. Disp. Sci. Technol.* **1994**, *15*, 513.

(40) Ammundsen, B.; Burns, G. R.; Jones, D. J.; Rozière, J. *J. Sol-Gel Sci. Technol.* **1997**, *8*, 331.

(41) Selle, M. H.; Sjöblom, J.; Friberg, S. E.; Young, T.; Yang, C. C. *Prog. Colloid Polym. Sci.* **1992**, *88*, 42.

Spectra were also recorded for model oxide compounds prepared as bulk phases by solid-state reactions. Model spinel compounds were $LiMn_2O_4$ (prepared from stoichiometric quantities of the corresponding carbonates at 800 °C), $LiMn_2O_{9/2}$ (reaction at 400 °C), and $Li_{4/3}Mn_{5/3}O_4$ (400 °C). The data for $LiMn_2O_4$ and $Li_{4/3}Mn_{5/3}O_4$ have been previously described.[30] The XANES and EXAFS spectra of the $LiMn_2O_{9/2}$ sample were essentially identical with those of $Li_{4/3}Mn_{5/3}O_4$, due to the similar manganese oxidation states and cation distributions in the two compounds. The Mn(III) oxide phase α-Mn_2O_3 was prepared by decomposition of β-MnO_2 (Aldrich, 98%) in air at 770 °C and γ-Mn_2O_3 by decomposition of λ-MnO_2 under vacuum at 200 °C. Manganese acetate tetrahydrate was used as a model for octahedrally coordinated Mn^{2+}. In all cases the phase purity was verified by XRD.

EXAFS and XANES Data Analysis. Experimental data were analyzed using the programs of Michalowicz.[42] XANES spectra were normalized to an edge jump of unity after removal of the background absorption by subtraction of a linear function extrapolated from the preedge. EXAFS spectra were normalized in the $\mu_{1,exp} - \mu_{0,exp}$ convention after simulating the atomic absorption $\mu_{0,exp}$ with third-order polynomials or spline functions. Fourier transformations using a Kaiser apodization window ($\tau = 3.5$) were performed over the k range 2.5−14 Å^{-1} using k^3 weighting to compensate for attenuation of the amplitude in the EXAFS spectra at high k.

Quantitative analyses of EXAFS spectra to determine R_i, the distance of the ith shell of atoms from the absorbing manganese atom, N_i, the number of atoms composing the shell, and σ_i, the Debye−Waller factor, were performed using curve-fitting procedures in k space after Fourier-filtering to isolate the EXAFS signal $\chi(k)$ corresponding to the relevant maxima in the Fourier transformations. Theoretical curves for Mn in the calcined gels were simulated using functions for the backscattering amplitude $F_i(k)$ and total phase shift $\phi_i(k)$ calculated for scattering paths by the ab initio XAS code FEFF6[43] using spinel lithium manganate and Mn_2O_3 as models.[30] For Mn in the solutions and gels before calcination, $F_i(k)$ and $\phi_i(k)$ for the Mn−O pair were calculated from the tabulated values of McKale et al.[44] Small adjustments for the energy origin E_0 ($1 < \Delta E_0 < 3$ eV) were introduced to optimize the fits. Agreement between experimental and theoretical curves over the k range 2.5−14 Å^{-1} gave statistical residues of less than 3% in most cases (residue $= \sum_k(k[\chi_{exp}(k)] - k[\chi_{th}(k)])^2k^3/\sum_k(k[\chi_{exp}(k)]^2)k^3$).

Results and Discussion

Materials Prepared from Ethanolic Gels. Before considering the surfactant-modified preparations, we briefly summarize the results obtained for the gels prepared in ethanol solutions. These gels, after drying at ambient temperature, produced shrunken brittle materials which were XRD amorphous. The materials were calcined at temperatures from 200 to 500 °C using different heating rates (1−10 °C/min), but in all cases, this resulted in XRD lines corresponding to α-Mn_2O_3 rather than a ternary lithium manganate phase. For higher metal nitrate content only, if the gels were rapidly heated to 500 °C a weak additional reflection appeared at ca. 18.5° 2θ indicating that a very small amount of spinel lithium manganate had also formed. Representative XRD patterns are shown in Figure 1 for ethanol gel prepared with 13 wt % nitrates and Li/Mn ratio 0.5, after calcinations at 400 and 500 °C. Increasing the concentration of lithium in the ethanolic gels to give a Li/Mn ratio of 2.0 produced no change, with peaks for α-Mn_2O_3 persisting as the dominant phase in XRD.

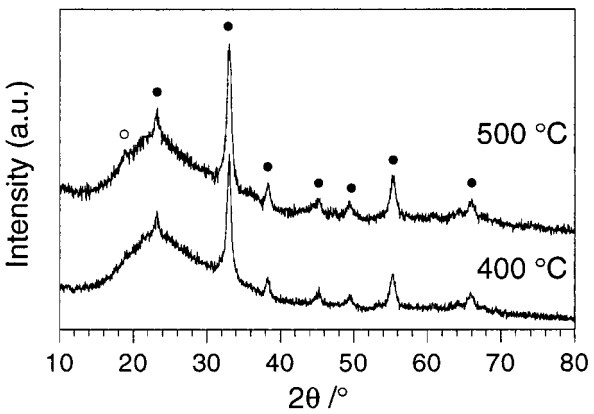

Figure 1. Powder XRD patterns of calcined ethanolic silica gels containing 13 wt % Li and Mn nitrates in molar ratio Li/Mn = 0.5. Peaks corresponding to α-Mn_2O_3 (●) and spinel (○) are marked.

While X-ray diffraction allows crystalline phases to be identified, poorly crystallized or amorphous phases in the materials are not detected. X-ray absorption spectroscopy, on the other hand, probes the average environment of a selected element, irrespective of whether the environment is crystallographically ordered. Figure 2 compares the manganese K-edge XANES, EXAFS, and Fourier-transformed EXAFS spectra of manganese in ethanolic gel (13 wt % nitrates, Li/Mn = 0.5) calcined at 400 °C with those of α-Mn_2O_3. The XANES spectrum of manganese in the calcined gel superimposes on that of the model, suggesting that the bulk of the manganese in the material is ordered α-Mn_2O_3 phase. This is confirmed by the EXAFS, where the Fourier transformed spectrum shows ordering corresponding to α-Mn_2O_3 up to coordination shells of ca. 7 Å radial distance. Figure 2d shows the simulated curve fitted to the EXAFS data Fourier-filtered over the range 1−4 Å for the calcined gel. The structural parameters produced by this simulation are given in Table 1 and show good agreement of Mn−O and Mn−Mn distances with those refined for the α-Mn_2O_3 model compound. Slightly lower coordination numbers and higher Debye−Waller factors for the calcined gel can be attributed to lower crystallinity than that of the model.

It can be concluded that a calcination temperature of 400 °C is sufficient to crystallize practically all of the manganese in the ethanolic gel as segregated α-Mn_2O_3, with little or no ternary lithium manganate forming. Microdomains of the crystalline phase were clearly visible by scanning electron microscopy at cleaved surfaces of the silica fragments, as shown in Figure 3. Similar results have been observed for ethanolic gels comprising magnesium and manganese nitrates where crystallization of Mn_2O_3 was also the main outcome of calcination, the magnesium ions remaining in the pores or being incorporated in the silica phase.[45]

Materials Prepared with the Surfactant C_{12}-$(EO)_4$. Gels prepared from solutions containing C_{12}-$(EO)_4$ were transparent and either colorless or faintly pink-tinted for high manganese nitrate content. Drying

(42) Michalowicz, A. In *Logiciels pour la Chimie*; Société Française de Chimie: Paris, 1991; p 102.

(43) Rehr, J. J.; Mustre de Leon, J.; Zabinsky, S. I.; Albers, R. C. *J. Am. Chem. Soc.* **1991**, *113*, 5135.

(44) McKale, A. G.; Veal, B. W.; Paulikas, A. P.; Chan, S.-K.; Knapp, G. S. *J. Am. Chem. Soc.* **1988**, *110*, 3763.

(45) Ammundsen, B.; Burns, G. R.; Amran, A.; Friberg, S. E. *J. Sol-Gel Sci. Technol.* **1995**, *4*, 23.

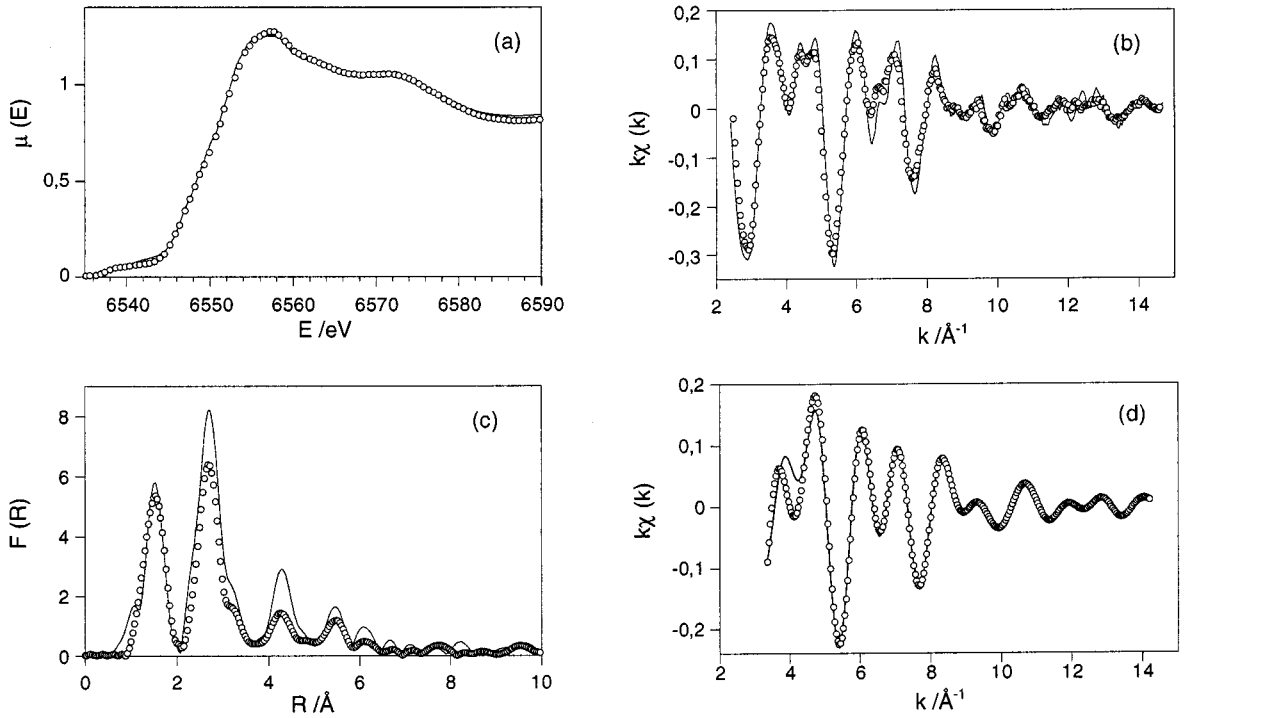

Figure 2. X-ray absorption data for Mn in ethanolic gel containing 13 wt % Li and Mn nitrates in molar ratio Li/Mn = 0.5 after calcination at 400 °C: (a) XANES, (b) EXAFS, and (c) Fourier-transformed EXAFS spectra (○) compared with spectra of model α-Mn_2O_3 (solid lines); (d) curve fit (solid line) to the Fourier-filtered EXAFS data for the calcined gel (○).

Table 1. Structural Parameters Derived from EXAFS Analyses of Mn Oxide Phase in Ethanolic Gel Calcined at 400 °C and Model α-Mn_2O_3

	gel phase			α-Mn_2O_3		
	R/Å	*N*	*σ*/Å	*R*/Å	*N*	*σ*/Å
Mn−O(1)	1.93	4.8[a]	0.057[b]	1.94	4.8[a]	0.041[c]
Mn−O(2)	2.11	1.2[a]	0.057[b]	2.12	1.2[a]	0.041[c]
Mn−Mn(1)	3.10	4.9	0.084	3.11	6[a]	0.082
Mn−Mn(2)	3.57	4.2	0.095	3.57	6[a]	0.086

[a] Parameters fixed. [b,c] Parameters linked.

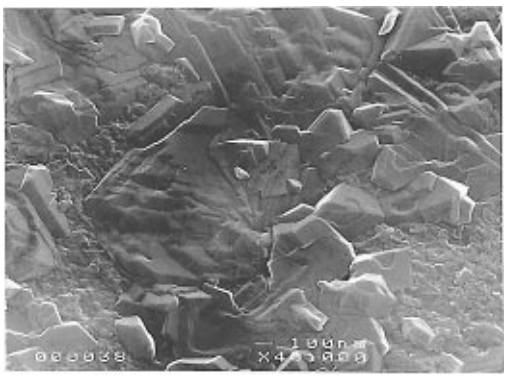

Figure 3. SEM photograph (40000*x* magnification) showing crystalline Mn_2O_3 in ethanolic silica gel calcined at 400 °C.

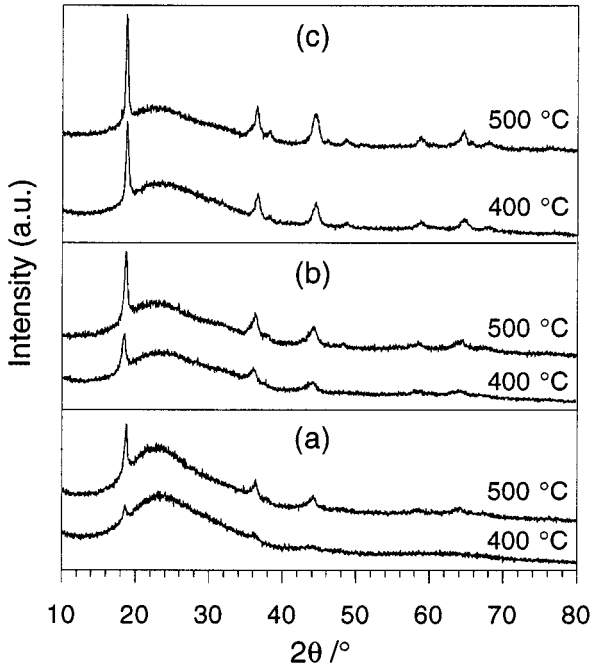

Figure 4. Powder XRD patterns for calcined $C_{12}(EO)_4$ silica gels containing (a) 8 wt % nitrate, molar ratio Li/Mn = 0.5, (b) 13 wt % nitrate, Li/Mn = 0.5, and (c) 15 wt % nitrate, Li/Mn = 2.

at ambient temperature resulted in only a small shrinkage of the monoliths compared with the ethanolic preparations, due to retention of the surfactant in the gel. The dried gels were XRD amorphous.

In contrast to the preparations in ethanol, gels prepared with $C_{12}(EO)_4$ presented XRD reflections uniquely for cubic spinel lithium manganate phase after calcination, with no evidence of crystalline Mn_2O_3. Figure 4 compares XRD patterns for samples after calcination at 400 and 500 °C, showing the results of changes in metal nitrate content and Li/Mn ratio. Unit cell parameters, estimated relative crystalline fractions, and average crystallite domain sizes calculated from the spinel patterns are given in Table 2. The relative crystalline fractions were estimated from the variation in the integrated intensity of the [111] line at ca. 18.5° 2θ, and domain sizes from the width of the [111] line using the Scherrer relation.[46] Calcining at 500 °C

(46) Scherrer, P. *Nachr. Göttinger Gesel. Dtsch.* **1918**, *2*, 98.

Table 2. Structural and Morphological Parameters for the Spinel Phase in Calcined $C_{12}(EO)_4$ Gels, Calculated from the XRD Data

		400 °C			500 °C		
metal salt (wt %)	Li/Mn ratio	a_0 (Å)	crystalline fraction[a]	crystallite size (nm)[b]	a_0 (Å)	crystalline fraction[a]	crystallite size (nm)[b]
8	0.5	8.21	0.19	19	8.20	0.40	25
13	0.5	8.22	0.32	20	8.22	0.60	26
15	2.0	8.16	0.70	21	8.16	1.00	27

[a] From the integrated intensity of the [111] line, normalized in arbitrary units with respect to the Li/Mn = 2 gel calcined at 500 °C. [b] From the width of the [111] line using the Scherrer relation.

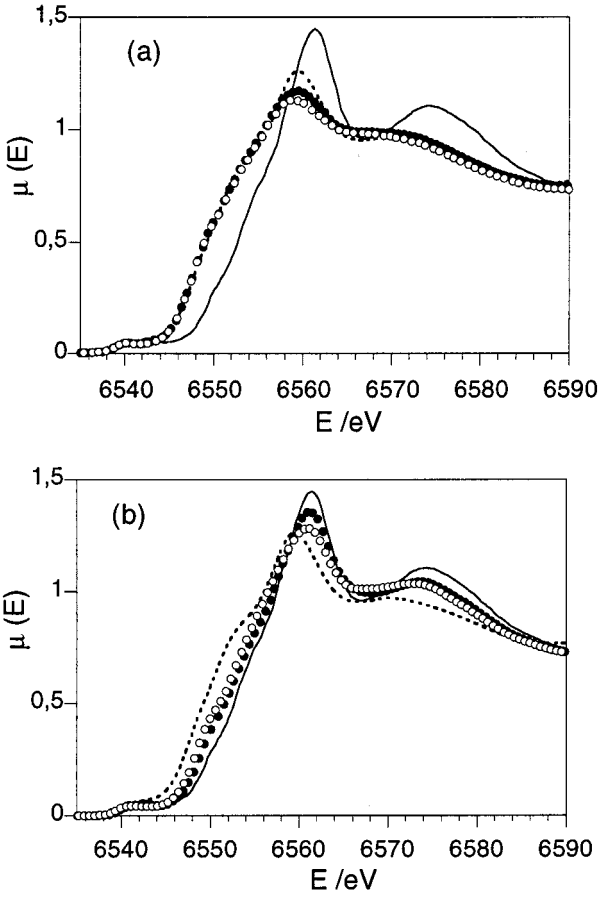

Figure 5. Mn XANES spectra of $C_{12}(EO)_4$ silica gels (a) containing 8 wt % (○) and 13 wt % (●) nitrates in molar ratio Li/Mn = 0.5 calcined at 400 °C and (b) 15 wt % nitrates, Li/Mn = 2, calcined at 400 °C (○) and 500 °C (●). Spectra of model compounds γ-Mn_2O_3 (dotted line) and $Li_{4/3}Mn_{5/3}O_4$ (solid line) are shown.

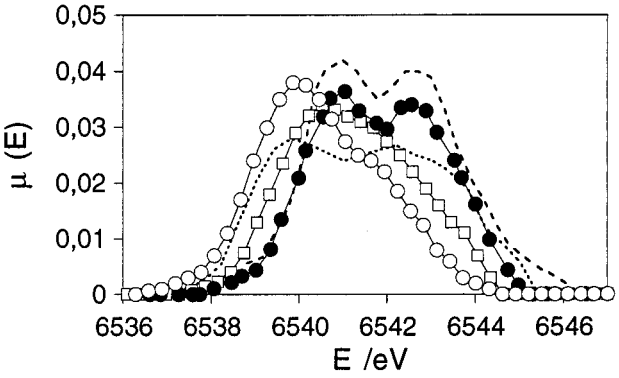

Figure 6. X-ray absorption preedge spectra of $C_{12}(EO)_4$ silica gel containing Li/Mn = 0.5 calcined at 400 °C (○), Li/Mn = 2 calcined at 400 °C (□), and Li/Mn = 2 calcined at 500 °C (●), compared with model compounds Mn_2O_3 (dotted line) and $Li_{4/3}Mn_{5/3}O_4$ (dashed line).

rather than 400 °C, increasing the total metal salt content in the gel, and including excess lithium all resulted in more intense XRD reflections, corresponding to increased fractions of crystalline lithium manganate phase. Significantly, however, although the diffraction lines change in intensity there is very little difference in the line width at half-height. This indicates that the higher quantities of crystalline lithium manganate result mainly from an increase in nucleation, giving a larger number of crystallites, rather than growth of the crystal domains.

Increasing the Li/Mn ratio in the $C_{12}(EO)_4$ gels also resulted in the formation of a spinel phase having a lower unit cell parameter, independent of the temperature of calcination. In bulk preparations of stoichiometric spinel $LiMn_2O_4$ the manganese has an average oxidation state of 3.5 and the unit cell parameter is typically ca. 8.24 Å.[9,47] Lower cell parameters result from an increased fraction of tetravalent manganese, compensated for by cation vacancies in the structure.[4] Such "cation-defect" spinels are typically prepared at temperatures between 400 and 700 °C and have cell parameters ranging between 8.17 and 8.22 Å.[47] It is also possible to prepare stoichiometric spinels in which a fraction x of the manganese is replaced by "excess" lithium in $Li_{1+x}Mn_{2-x}O_4$, in the range $0 < x < 0.33$.[10] In these compounds the average manganese oxidation state also tends toward tetravalent and the unit cell parameters may be as low as 8.14 Å.[47] The cell parameter of 8.16 Å for the Li/Mn = 2 material in Table 2 indicates the formation of a highly cation-defect or $Li_{1+x}Mn_{2-x}O_4$ phase.

Figure 5 compares Mn XANES spectra of calcined $C_{12}(EO)_4$ gels with the model compounds $Li_{4/3}Mn_{5/3}O_4$ and γ-Mn_2O_3. The spectra of spinel lithium manganates are characterized by a double inflection in the rising absorption edge and two strong resonances above the edge. These features result from multiple scattering of the photoelectron in highly degenerate paths contained within a small spinel cluster of ca. 3.5 Å radius around the absorbing manganese atoms.[30,48] Similar features, although weaker, are observed in the spectrum of γ-Mn_2O_3, which has a disordered spinel structure. The absorption edge also provides information concerning manganese oxidation state: the edge for $Li_{4/3}Mn_{5/3}O_4$ (Z_{Mn} ca. 3.9[30]) lies ca. 4 eV higher in energy than that of γ-Mn_2O_3 ($Z_{Mn} = 3.0$).

For the Li/Mn = 0.5 gels calcined at 400 °C (Figure 5a), the edge spectra consist of a broad and featureless edge jump at the Mn^{3+} position. The postedge resonances are also broad. It can be concluded that although XRD shows a small fraction of crystalline

(47) Le Cras, F.; Strobel, P.; Anne, M.; Bloch, D.; Soupart, J.-P.; Rousche, J.-C. *Eur. J. Solid State Inorg. Chem.* **1996**, *33*, 67.
(48) Ammundsen, B.; Jones, D. J.; Rozière, J. *J. Phys. IV* **1997**, *7*, 1257.

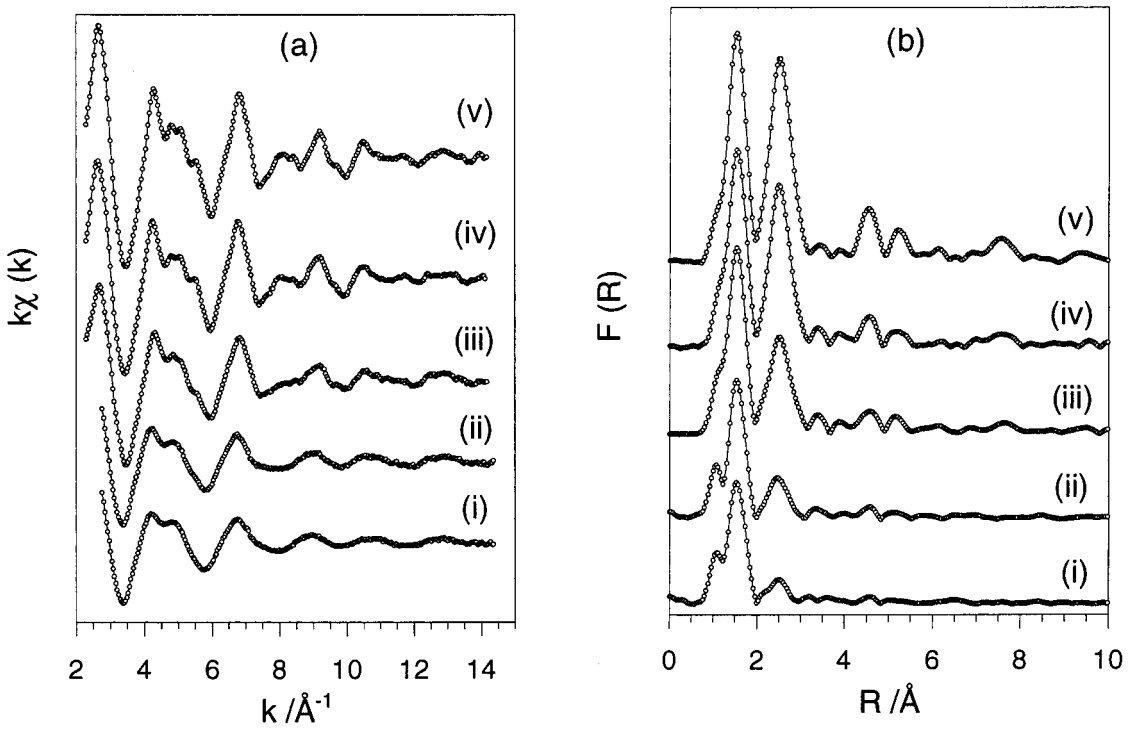

Figure 7. (a) EXAFS and (b) Fourier-transformed spectra of $C_{12}(EO)_4$ silica gel containing (i) 8 wt % nitrates in molar ratio Li/Mn = 0.5 calcined at 400 °C, (ii) 13 wt % nitrates Li/Mn = 0.5 (400 °C), (iii) 15 wt % nitrates Li/Mn = 2 (400 °C), and (iv) 15 wt % nitrates Li/Mn = 2 (500 °C), compared with (v) model $Li_{4/3}Mn_{5/3}O_4$ spinel.

lithium manganate in these samples, most of the manganese has remained in a structurally disordered environment and in a low oxidation state. However when the Li/Mn ratio in the gel is 2.0 (Figure 5b), XANES characteristic of spinel ordering appears at 400 °C and is further evolved after calcination at 500 °C. The edges also move to higher energy for the Li/Mn = 2 samples, and the postedge resonances correlate in position with the $Li_{4/3}Mn_{5/3}O_4$ model. The increase in Li/Mn ratio and calcination temperature therefore result in more extensive medium-range ordering of spinel phase in the average manganese environment and produce a higher content of tetravalent manganese, in agreement with the conclusions from XRD.

The preedge X-ray spectra for these samples are shown in more detail in Figure 6, base line corrected by subtracting the extrapolated tail of the absorption edge. The peaks observed derive from transitions to bound electronic states in the $[MnO_6]$ octahedra and their energies therefore provide a reliable indication of manganese oxidation state in the samples.[30] For the Li/Mn = 0.5 gels calcined at 400 °C the spectral contribution to the preedge appears to be dominated by Mn^{3+}, agreeing with the observed main edge position. The increased Li/Mn ratio results in a displacement of the preedge to higher energy, and after calcination at 500 °C, the dominant contribution to the spectrum corresponds to the Mn^{4+} peaks observed in the preedge of $Li_{4/3}Mn_{5/3}O_4$.

Figure 7 shows the EXAFS spectra of the calcined C_{12}-$(EO)_4$ materials and their Fourier transformations, compared with the $Li_{4/3}Mn_{5/3}O_4$ model. The structural origins of the EXAFS are schematically represented in Figure 8, which shows the local structure around a manganese ion in spinel lithium manganate. The EXAFS spectrum of $Li_{4/3}Mn_{5/3}O_4$ is characterized by dominant contributions from simple photoelectron back-

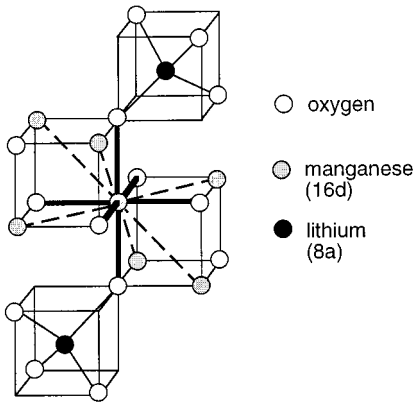

Figure 8. Schematic diagram of the local structure around a manganese ion in spinel lithium manganate. Bonds to oxygens in the first coordination shell are represented by heavy solid lines, dashed lines indicate photoelectron backscattering paths to neighboring manganese ions which form the second coordination shell.

scattering by the first regular octahedral coordination shell of six oxygens and a second coordination shell composed of ca. five nearest neighbor manganese ions in edge-sharing octahedra. The tetrahedral (8a) sites in spinel lithium manganate are occupied by lithium only, which contributes insignificantly to the XAFS. Other significant contributions to the spectrum derive only from manganese ions ordered in coherent shells at ca. 4.8 and 5.6 Å.

The EXAFS spectra of Figure 7 show that higher metal salt content, Li/Mn ratio, and calcination temperature result in increased order in the average manganese environment. The ordering of manganese shells contributes increasing fine structure to the EXAFS and appears as increasingly intense maxima at R = 2.5, 4.5, and 5.3 Å in the (non phase-corrected) Fourier transformed data. In each case curve-fitting was per-

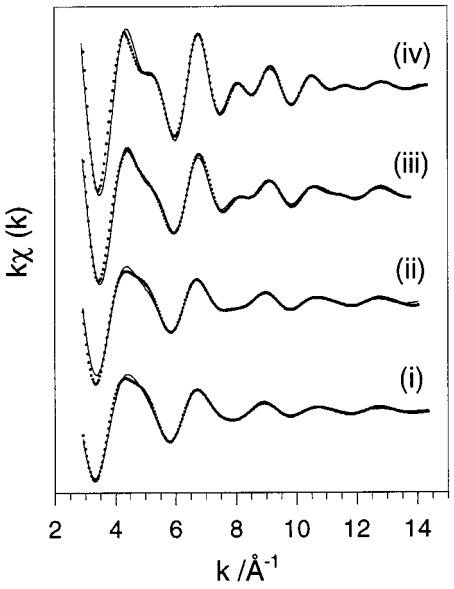

Figure 9. Curve fits (solid lines) to the Fourier-filtered EXAFS data (points) for $C_{12}(EO)_4$ silica gel containing (i) 8 wt % nitrates in molar ratio Li/Mn = 0.5 calcined at 400 °C, (ii) 13 wt % nitrates Li/Mn = 0.5 (400 °C), (iii) 15 wt % nitrates Li/Mn = 2 (400 °C), and (iv) 15 wt % nitrates Li/Mn = 2 (500 °C).

Table 3. Structural Parameters Derived from EXAFS Analyses of Mn Oxide Phases in Calcined $C_{12}(EO)_4$ Gels Compared with $Li_{4/3}Mn_{5/3}O_4$

	i	N_i[a]	R_i/Å	σ_i/Å
Li/Mn = 0.5 (8 wt %) 400 °C	O	4.2	1.91	0.081
	O	1.8	2.26	0.109
	Mn	1.2	2.90	0.104
Li/Mn = 0.5 (13 wt %) 400 °C	O	4.2	1.91	0.067
	O	1.8	2.14	0.098
	Mn	1.9	2.90	0.094
Li/Mn = 2 (15 wt %) 400 °C	O	4.9	1.91	0.059
	O	1.1	2.14	0.067
	Mn	3.2	2.88	0.089
Li/Mn = 2 (15 wt %) 500 °C	O	6	1.91	0.055
	Mn	4.4	2.88	0.084
$Li_{4/3}Mn_{5/3}O_4$	O	6	1.91	0.066
	Mn	5.1	2.87	0.077

[a] $\Sigma N_O = 6$.

formed to the data Fourier-isolated over the range 0.9−3.1 Å to obtain structural parameters for the first oxygen and manganese shells. The curve fits are shown in Figure 9, and the structural data are reported in Table 3. An important aspect of the curve-fitting refinements for the gel phases was that the first coordination shell could not always be satisfactorily fitted using a single Mn−O distance. For the Li/Mn = 0.5 materials calcined at 400 °C, the Fourier-isolated oscillations show significant asymmetry and were best simulated using two Mn−O distances corresponding to a distorted octahedral environment resembling that found in γ-Mn_2O_3. The results are consistent with the Jahn−Teller distortion found for Mn^{3+} in octahedral coordination. The asymmetry in the Mn−O shell was much less for the Li/Mn = 2.0 materials, agreeing with the higher average oxidation state of manganese in these materials. As the degree of local spinel order increases, the average Mn−O distances also become shorter and the Debye−Waller factors lower, indicating the removal of spectral contributions from Mn^{3+}.

The EXAFS data support the powder XRD observations in confirming that spinel lithium manganate is the

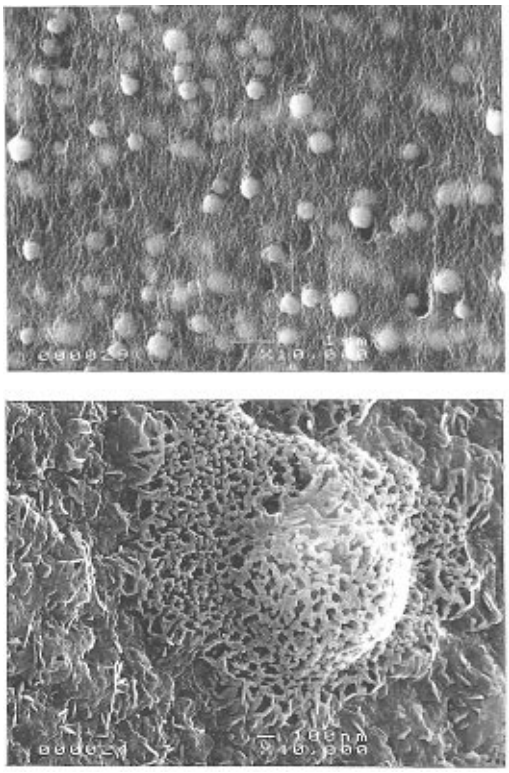

Figure 10. SEM photographs showing microstructure of metal oxide phase in $C_{12}(EO)_4$ Li/Mn = 0.5 gels after calcination at (a, top) 300 °C (10000× magnification) and (b, bottom) 400 °C (40000× magnification).

unique ordered phase in the calcined $C_{12}(EO)_4$ materials. The Mn−Mn distances are consistent with this structure, and no signal is detected between 3 and 4 Å which would indicate manganese in corner-sharing octahedra or ordered Mn(III) oxide phase. In the Li/Mn = 0.5 gels calcined at 400 °C, the low coordination numbers obtained for the nearest neighbor manganese shell are due to local structural disorder and lack of coherence in Mn−Mn distances, manifested in XRD as low crystalline fraction. X-ray absorption shows the average manganese environments in the samples, and Mn^{3+} present in a disordered environment will contribute little to the EXAFS beyond the first coordination shell of oxygen atoms. In contrast, the number of nearest manganese neighbors for the Li/Mn = 2.0 gel calcined at 500 °C approaches the value observed for $Li_{4/3}Mn_{5/3}O_4$, indicating that practically all the manganese in the gel has reacted to form lithium manganate phase. Furthermore the Mn−Mn distances determined from the EXAFS correlate better with a $Li_{4/3}Mn_{5/3}O_4$ or $LiMn_2O_{9/2}$ model than with $LiMn_2O_4$, for which $R_{Mn-Mn} \approx 2.91$ Å.[30] This is again in accordance with the XRD data in indicating that the lithium manganate phase contains a high proportion of tetravalent manganese and has either vacancies or lithium ions on a fraction of the octahedral sites.

Scanning electron microscopy (SEM) showed two different morphologies for metal oxide phase in these gels. For samples with Li/Mn = 0.5, open branched clusters of metal oxide are observed distibuted throughout the bulk of the silica fragments, as shown in Figure 10. Individual particles in these clusters are ca. 20 nm in diameter. For the Li/Mn = 2 sample these spherical clusters are not observed, but after calcination at 400−

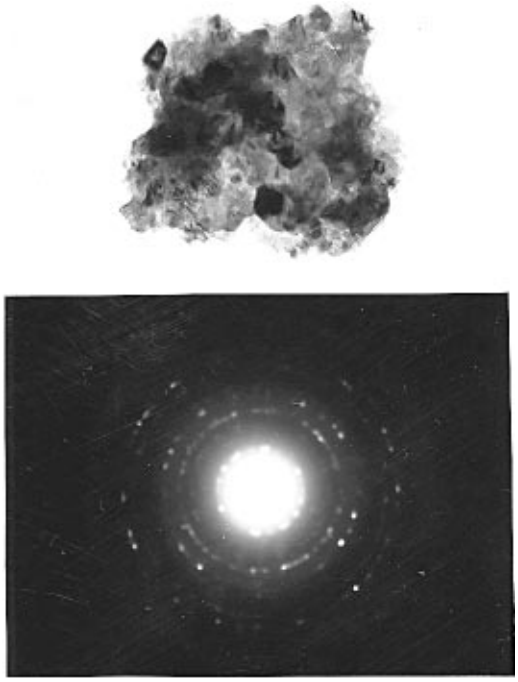

Figure 11. (a, top) TEM photograph (105000× magnification) of an isolated (poly)nanocrystalline particle from $C_{12}(EO)_4$ Li/Mn = 2 gel after calcination at 500 °C and (b, bottom) selected area electron diffraction confirming the spinel lithium manganate structure.

500 °C the silica fragments are covered by crystalline metal oxide particles with a platey morphology penetrating into the interior of the fragments up to a depth of several microns. Particles of this sample isolated for transmission electron microscopy (TEM) are polycrystalline with average crystallite dimensions of ca. 25−30 nm, agreeing well with the domain size calculated from XRD, and produce selected area electron diffraction patterns for spinel lithium manganate (Figure 11).

The observations imply that the surfactant, interacting with the metal salt in the silica gels, may influence the morphology and dispersion of the metal oxide phase at two different scales. At the first level, the surfactant suppresses crystallization during calcination of large domains of α-Mn_2O_3 such as that observed for equivalent metal nitrate contents in ethanolic gels and gives instead a nanocrystalline spinel lithium manganate phase. At a second level, the nanocrystalline phase is organized into microstructures which suggest that the surfactant in the gels assembles metal ions in specific arrangements which depend at least partly on the ionic concentration. Further evidence for formation of specific microstructures by self-organization of the surfactant component of the gel is considered in the following section.

Influence of the Nature of the Surfactant. Gels prepared by replacing the $C_{12}(EO)_4$ with equivalent weight percent of $C_{12}\phi(EO)_5$, $C_{17}C{=}O(EO)_5$, or ethylene glycol were all monolithic and XRD amorphous. Calcination of these gels at 400−500 °C resulted exclusively in diffraction lines for lithium manganates. Single-phase spinels are obtained for preparations with $C_{12}\phi(EO)_5$ and ethylene glycol for Li/Mn ratios up to 2. XRD patterns for a given composition are essentially identical with those given by the $C_{12}(EO)_4$ gels after calcination at equivalent temperatures, indicating similar trends in crystallization and crystallite size as a function of metal nitrate content, Li/Mn ratio, and calcination temperature. Preparations with $C_{17}C{=}O(EO)_5$ show slightly different behavior in that raising the Li/Mn ratio above 1, and calcining at 500 °C results in the appearance of diffraction lines for the rock salt phase Li_2MnO_3. This is consistent with results for bulk preparations (in the absence of silica) where Li_2MnO_3 always appears in samples with Li/Mn > 0.8[47] and implies that $C_{17}C{=}O(EO)_5$ favors stoichiometric reaction between lithium and manganese to a greater extent than the other surfactants studied. The XRD lines for the $C_{17}C{=}O(EO)_5$ samples also have consistently narrower widths at half-maximum than the other calcined gels, implying the formation of larger crystallites, e.g., of the order of 30−40 nm at 500 °C. XANES and EXAFS in all cases show the presence of large proportions of Mn^{3+} in disordered environments for gels calcined at 400 °C or below, but characteristic increases in both manganese oxidation state and long-range order when lithium manganate phase is more extensively crystallized.

It may therefore be inferred that, apart from the differences observed for $C_{17}C{=}O(EO)_5$, the nature of the poly(oxyethylene) surfactant has little influence on the reaction between lithium and manganese to form the ternary oxide phase. Indeed the same result is achieved even when the surfactant is replaced by ethylene glycol. However, differences in the morphology and dispersion of the lithium manganate are obtained by varying the surfactant. In the case of preparations using $C_{12}\phi(EO)_5$, crystals of cubic morphology appear at the surface of the silica fragments, while the interiors of the fragments contain clusters of platey and needlelike particles. Better dispersion of the metal oxide phase was achieved with $C_{17}C{=}O(EO)_5$, where 30 wt % surfactant in the gels allows formation of uniformly distributed "worm-like" particles of lithium manganate in the bulk silica, shown in Figure 12. The importance of the surfactant component in determining the morphology can be emphasized here, as using lower concentrations of $C_{17}C{=}O(EO)_5$ gave rise to a less controlled morphology with the appearance of disordered domains of platey phase.

Different forms of surfactant self-organization are therefore the probable origins of the differences in microstructure observed when the surfactant is varied. Significant supporting evidence for microstructure formation by surfactant assembly is obtained by comparisons with the ethylene glycol preparations. Ethylene glycol differs from the poly(oxyethylene) surfactants in having no amphiphilic character; therefore, although it may form complexes with metal ions, it is not expected to form micellar type structures. Calcination of the ethylene glycol gels produced materials in which crystallization of lithium manganate occurs only at the surfaces of the fragmented monoliths. The interior parts of the fragments are amorphous and finely particulate in appearance, with no heterogeneous structure of the type seen in the surfactant preparations.

Manganese XAFS of Gels before Calcination. The environment of the metal ions in the as-prepared gels is expected to be an important factor in determining the structures obtained by calcination. However, infrared spectroscopy provides little information because intense bands due to vibrations of the surfactant oxy-

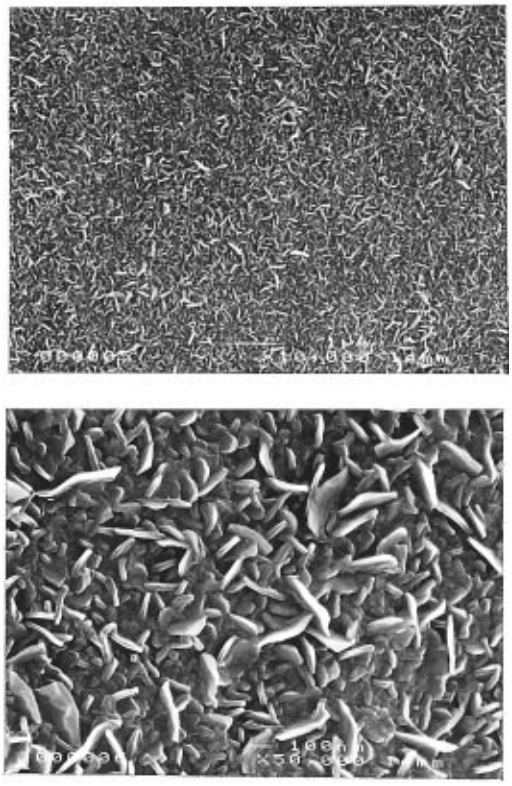

Figure 12. SEM photographs showing microstructure of metal oxide phase in $C_{17}C{=}O(EO)_5$ Li/Mn = 0.5 gel after calcination at 500 °C: (a, top) 10000× magnification, (b, bottom) 50000× magnification.

ethylene ether linkages between 1000 and 1200 cm^{-1} overlap with absorption due to Si−O stretching and absorption due to silanol groups obscures the terminal O−H stretch of the surfactants and ethylene glycol. In the electronic spectra, the weak absorption bands due to the d_5 Mn^{2+} ions are swamped by absorption by the nitrate and organic components. We therefore recorded X-ray absorption data for manganese nitrate dissolved in ethanolic solutions of surfactant or ethylene glycol and for different gels after drying at ambient temperature. XANES spectra are shown for solutions and gels in Figure 13, and EXAFS spectra for gels are shown in Figure 14.

In all cases the XANES spectra of manganese in the gels are identical with those of manganese ions in solution where there is no order beyond the first coordination shell.[49] However, comparison of the absorption edge and preedge regions shows that the chemical environments of manganese in the surfactant and ethylene glycol/silica matrixes are different from the gel prepared in simple ethanol solution. The differences are most easily observed in the first derivative curves of the XANES spectra. Whereas the spectrum for manganese in the ethanol gel is identical with that of the hexaaquo ion $[Mn(OH_2)_6]^{2+}$ in solution,[49,50] the absorption edges of manganese in the surfactant and ethylene glycol systems are slightly displaced to higher energy relative to the ethanol gel, indicating some partial oxidation of the manganese ions. In the derivative curves, this appears as the evolution of a new peak corresponding to a higher-energy inflection in the absorption edge. A modification of the electronic environment of the manganese in the surfactant and ethylene glycol systems is also indicated by the preedge peaks, which become both broader and shifted to slightly higher energy from the solutions to the dried gels.

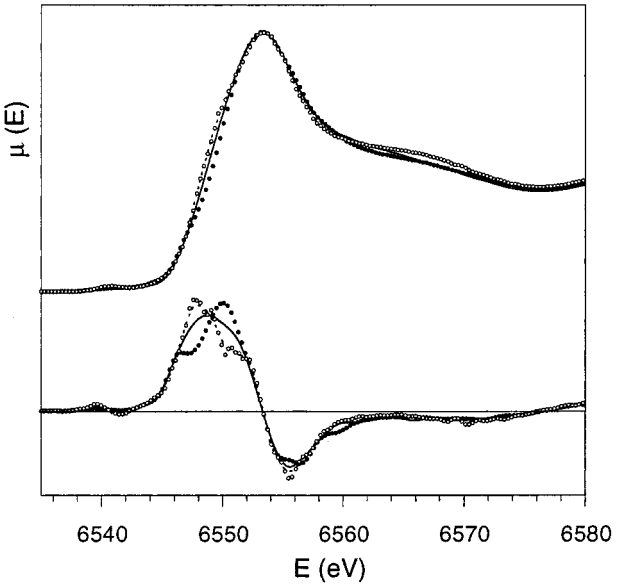

Figure 13. XANES spectra and first derivatives of Mn in ethanolic gel (○) and $C_{12}(EO)_4$ gel (●) before calcination, compared with Mn dissolved as the nitrate salt in aqueous solution (dotted line) and in an ethanol solution of $C_{12}(EO)_4$ (solid line). Spectra recorded for ethylene glycol gel and solution were identical with those for $C_{12}(EO)_4$.

The corresponding EXAFS spectra show contributions from the first coordination shell only. The structural parameters obtained by curve-fitting for this shell, given in Table 4, show coordination by six oxygens in each case with average Mn−O distances of 2.18−2.19 Å, consistent with divalent manganese. However higher Debye−Waller factors in the case of the surfactant and ethylene glycol gels imply a greater distribution in Mn−O bond lengths, as would be expected with the presence of different species in the coordination environment. Correlating the EXAFS results with the XANES observations, it can be concluded that manganese ions in the surfactant and ethylene glycol gel materials are predominantly associated with the interstitial organic components.

Mechanisms of Lithium Manganate Formation and Microstructure. XAFS and XRD show that while little or no reaction between lithium and manganese occurs in gels prepared in simple ethanol solutions, preparing the gels in solutions of poly(oxyethylene) surfactants or ethylene glycol both suppresses the crystallization of segregated manganese oxide and promotes the nucleation of ternary lithium manganate. We have previously shown that calcination at 400 °C is sufficient to crystallize practically all the manganese in a conventionally prepared ethanol gel as α-Mn_2O_3 but that gels prepared with poly(oxyethylene) surfactant and manganese nitrate remain mostly amorphous.[40] The inclusion of a lithium salt in the surfactant gels therefore has the effect of "activating" crystallization of the manganese as the ternary oxide.

(49) Belli, M.; Bianconi, A.; Burattini, E.; Mobilio, S.; Palladino, L.; Reale, A.; Scarfati, A. *Solid State Commun.* **1980**, *35*, 355.
(50) Garcia, J.; Bianconi, A.; Benfatto, M.; Natoli, C. R. *J. Phys. Colloq.* **1986**, *47*, C-8 49.

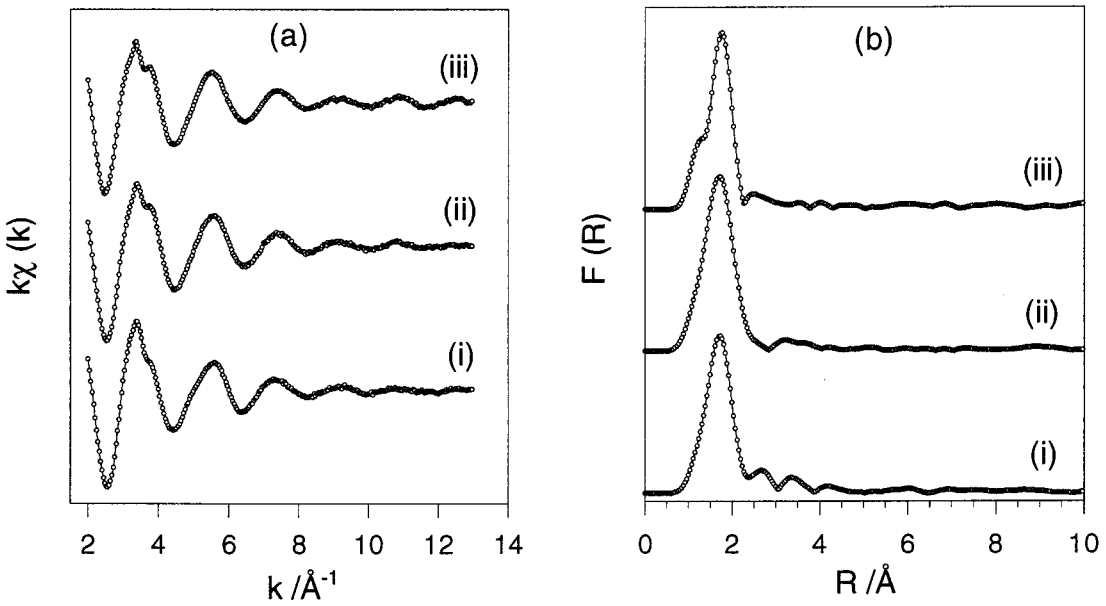

Figure 14. (a) EXAFS and (b) Fourier-transformed spectra of (i) $C_{12}(EO)_4$, (ii) ethylene glycol, and (iii) ethanolic gels before calcination.

Table 4. EXAFS Interatomic Distances and Debye−Waller Factors for the MnO_6 Species in the Gels and in Manganese Acetate Tetrahydrate

	R/Å	*σ*/Å
$C_{12}(EO)_4$ gel	2.18	0.090
ethylene glycol gel	2.19	0.084
ethanolic gel	2.18	0.072
manganese acetate tetrahydrate	2.19	0.071

These results imply that the most important factor for formation of the ternary oxide is the ability of the poly(oxyethylene) or glycol component in the interstitial liquid of the gels to assemble lithium and manganese ions prior to calcination. Such assembly using glycols followed by pyrolysis of the organic component has been used in the preparation of lithium manganate as a bulk phase.[51] In the composite gels prepared here, binding of metal ions by the ether linkages or glycol oxygens of the incorporated organic component should favor the nucleation of small crystalline particles of ternary oxide phase and prevent large-scale colloidal segregation of the salts in the pores.

Association between the metal ions and the surfactant molecules results in a diversity of microstructures after calcination. It is well-known that silica or other alkoxide-derived hydrous oxides may be precipitated or polymerized in surfactant-stabilized microemulsions or lyotropic liquid crystals, allowing control over particle size, texture, and porosity.[52−57] Recent developments in this area include the preparation of monolithic silica materials formed in periodic lamellar, hexagonal, and cubic arrays of poly(oxyethylene) surfactant.[58] However, the preparation of the gels described in the present work differs from these systems because ethanol liberated by the hydrolysis of TEOS destroys the periodic order of surfactant assemblies and gives isotropic solutions.[40,41] The monolithic gels were allowed to form without removing the evolved ethanol from the solutions, and only after aging of the gels in sealed containers was ethanol permitted to evaporate. Periodic structure was therefore not present in the silica matrixes, as confirmed by the absence of low-angle diffraction peaks in XRD.

Nevertheless, some self-assembly among the surfactant molecules in the gels is expected, with the possibility of further structural evolution when ethanol is evaporated after gelation. Because the volume fraction of surfactant in the gels is high, microdomains of surfactant and metal salt may form within the polymerized silica matrix, determining the morphology of the metal oxide phase obtained by calcination. Furthermore, the interaction of the ionic salts with the surfactant component may in itself influence the formation of amphiphilic structures in the gels. The affinity of poly(oxyethylene)-type molecules for metal salts may therefore be combined with their amphiphilic properties to produce a range of novel microstructures.

Conclusions

The work presented here demonstrates the potential for preparing nanocomposite materials of metal oxide and silica with controlled morphology by combining the chemical and self-assembly properties of poly(oxyethylene) surfactants. First, the method allows the preparation of nanocrystalline lithium manganate in a silica matrix, which cannot be prepared by conventional sol−gel processing in alcoholic media. Investigations of the

(51) Schleich, D. M. *Solid State Ionics* **1994**, *70&71*, 407.
(52) Osseo-Asare, K.; Arriagada, F. J. *Colloids Surf.* **1990**, *50*, 321.
(53) Burban, J. H.; He, M.; Cussler, E. L. *AIChE J.* **1995**, *41*, 159.
(54) Friberg, S. E.; Ma, Z. *J. Non-Cryst. Solids* **1992**, *147&148*, 30.
(55) Guizard, C.; Stitou, M.; Larbot, A.; Cot, L.; Rouvière, J. In *Better Ceramics Through Chemistry III*; Brinker, C. J., Clark, D. E., Ulrich, D. R., Eds.; Materials Research Society: Pittsbugh, 1988; p 115.
(56) Beck, J. S.; Vartuli, J. C.; Roth, W. J.; Leonowicz, M. E.; Kresge, C. T.; Schmitt, K. D.; Chu, C. T.-W.; Olson, D. H.; Sheppard, E. W.; McCullen, S. B.; Higgins, J. B.; Schlenker, J. L. *J. Am. Chem. Soc.* **1992**, *114*, 10834.
(57) Dabadie, T.; Ayral, A.; Guizard, C.; Cot, L.; Lacan, P. *J. Mater. Chem.* **1996**, *6*, 1789.
(58) Attard, G. S.; Glyde, J. C.; Göltner, C. G. *Nature* **1995**, *378*, 366.

lithium extraction and insertion reactions of these phases are currently under way. Second, different microstructures can be produced by changing the nature of the surfactant. The complex compositions of the solutions and gels, in particular the high salt concentrations and the disordering influence of ethanol produced in the reaction systems, make it difficult to relate the microstructural differences in the final materials to the more generally known phase behavior of the surfactants in simple solutions. However key differences between the preparations have been identified and will be used as a basis to further develop this class of new tailored materials.

Acknowledgment. The authors thank the CEA-CNRS-MENESR for access to the facilities at LURE, Françoise Villain (LURE) for assisting with X-ray absorption experiments, and Lucien Datas (Laboratoire de Microscopie Electronique, UM2) for scanning electron microscopy. B.A. thanks the French Ministère des Affairs Etrangères for support to conduct work in France through the France−New Zealand Cultural Agreement and the New Zealand Foundation for Research, Science and Technology for the award of a postdoctoral fellowship in 1997−1998.

CM9705698